JOURNAL OF GEOPHYSICAL RESEARCH, VOL. 113, A00A11, doi:10.1029/2008JA013222, 2008

Three-dimensional reconstructions of the early November 2004 Coordinated Data Analysis Workshop geomagnetic storms: Analyses of STELab IPS speed and SMEI density data

M. M. Bisi,[1] B. V. Jackson,[1] P. P. Hick,[1] A. Buffington,[1] D. Odstrcil,[2,3] and J. M. Clover[1]

Received 2 April 2008; revised 12 June 2008; accepted 18 July 2008; published 21 October 2008.

[1] Combined interplanetary scintillation (IPS) and Solar Mass Ejection Imager (SMEI) remote-sensing observations provide a view of the solar wind at almost all heliographic latitudes and covering distances from the Sun between 0.1 AU and 3.0 AU. They are used to study the development of the solar wind and coronal transients as they move out into interplanetary space, and also the inner heliospheric response to the passage of corotating solar structures and coronal mass ejections (CMEs). The observations take place in both radio scintillation level and speed for IPS, and in Thomson-scattered white light brightness for SMEI. With colleagues at the Solar Terrestrial Environment Laboratory (STELab), Nagoya University, Japan, we have developed a data analysis system for the STELab IPS data which can also be applied to SMEI white light data. This employs a three-dimensional (3-D) reconstruction technique that obtains perspective views from solar corotating plasma and outward flowing solar wind as observed from the Earth by iterative fitting of a kinematic solar wind model to the data. This 3-D modeling technique permits reconstructions of the density and speed of CMEs and other interplanetary transients at relatively coarse spatial and temporal resolutions. For the time-dependent model (used here), these typically range from 5° to 20° in latitude and longitude, with a 1/2 to 1 day time cadence. For events during early November 2004 we compare these reconstructed structures with in situ measurements from the ACE and Wind (near-Earth) spacecraft to validate the 3-D tomographic reconstruction results and provide input to the ENLIL 3-D magnetohydrodynamic (MHD) numerical model.

Citation: Bisi, M. M., B. V. Jackson, P. P. Hick, A. Buffington, D. Odstrcil, and J. M. Clover (2008), Three-dimensional reconstructions of the early November 2004 Coordinated Data Analysis Workshop geomagnetic storms: Analyses of STELab IPS speed and SMEI density data, *J. Geophys. Res.*, *113*, A00A11, doi:10.1029/2008JA013222.

1. Introduction

[2] This paper uses interplanetary scintillation (IPS) data from the Solar Terrestrial Environment Laboratory (STELab) [e.g., *Kojima and Kakinuma*, 1987] at 327 MHz and from the Solar Mass Ejection Imager (SMEI) [*Eyles et al.*, 2003; *Jackson et al.*, 2004] taken during October/November 2004 (Carrington rotations 2022.5–2023.5), and compares these with in situ measurements from the Advanced Composition Explorer - Solar Wind Electron, Proton and Alpha Monitor (ACE|SWEPAM) [*Stone et al.*, 1998; *McComas et al.*, 1998] and the Wind - Solar Wind Experiment (Wind|SWE) [*Ogilvie and Desch*, 1997; *Ogilvie et al.*, 1995].

[3] IPS has been used for solar wind observations for over 40 years. It is the rapid variation in signal received by radio antennas on Earth from a compact radio source, arising from scattering by small-scale (~150 km) density inhomogeneities in the solar wind. IPS observations allow the solar wind speed to be inferred over all heliographic latitudes and a wide range of heliocentric distances (dependent upon source strength and observing frequency) [e.g., *Hewish et al.*, 1964; *Coles and Maagoe*, 1972; *Rickett*, 1992; *Fallows et al.*, 2002, 2006; *Bisi et al.*, 2005, 2007]. When two or more radio telescopes are used and the separation of the raypaths in the plane of the sky from source to each telescope lies close to radial (the solar wind flow direction) centered at the Sun, a high degree of correlation between the patterns of scintillation recorded at the two telescopes may be observed [e.g., *Armstrong and*

[1]Center for Astrophysics and Space Sciences, University of California, San Diego, La Jolla, California, USA.
[2]Cooperative Institute for Research in Environmental Sciences, University of Colorado, Boulder, Colorado, USA.
[3]Space Weather Prediction Center, National Oceanic and Atmospheric Administration, Boulder, Colorado, USA.

0148-0227/08/2008JA013222$09.00

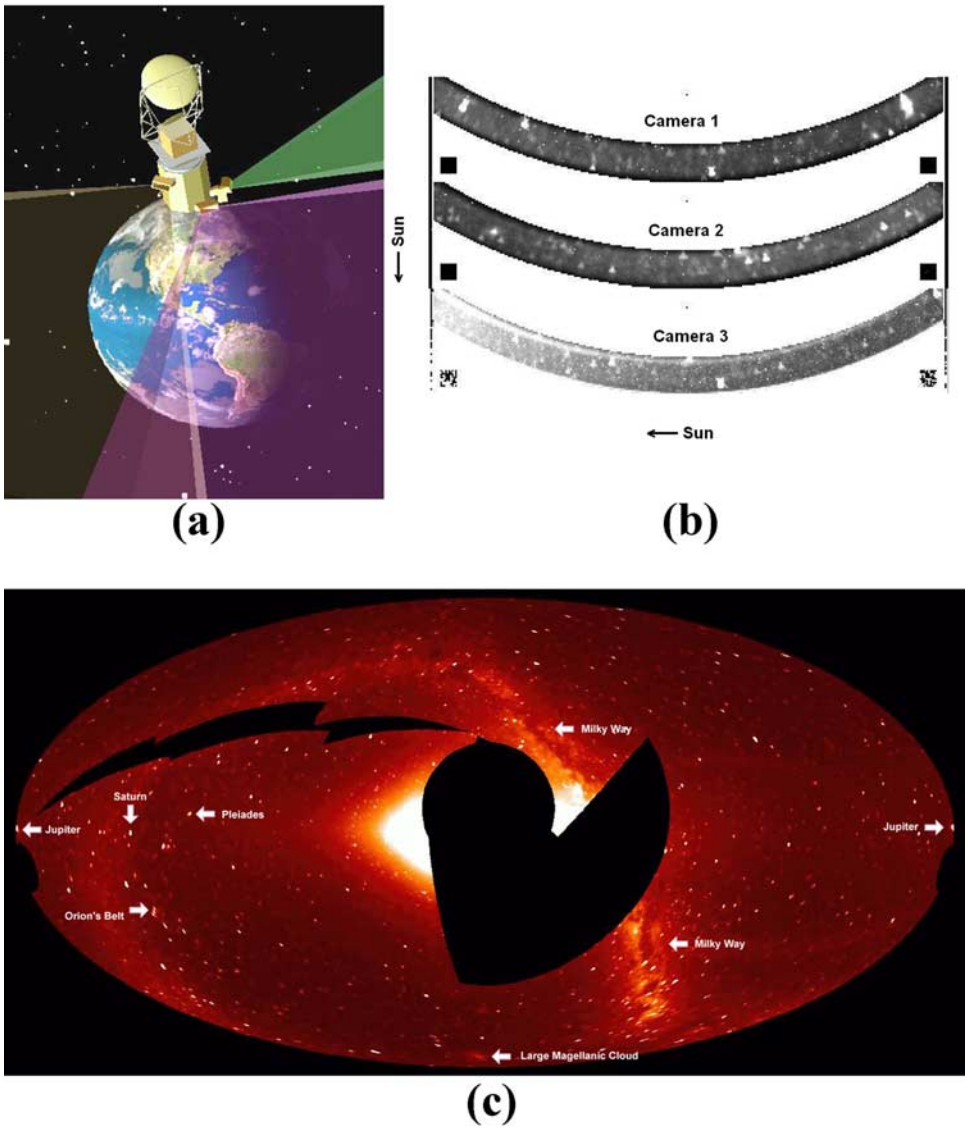

Figure 1. A summary of the Solar Mass Ejection Imager (SMEI) setup. (a) An artist's impression of the SMEI instrument aboard the Coriolis satellite in its zenith-nadir-pointing polar orbit at 840 km altitude with an inclination of 98° [*Jackson et al.*, 2004]. The field of view covered by each of the three cameras is highlighted showing a near-all-sky coverage with some overlap. SMEI looks away from the Earth above the horizontal by an angle of 30° in order to avoid Earth-reflected sunlight. (b) Three 60° image frames from the SMEI instrument [*Jackson et al.*, 2004]. The top image (Camera 1) is a view at the largest elongation away from the Sun, and the bottom image (Camera 3) is a view closest to the Sun. The Sun is to the left in each camera view. (c) SMEI first light combined Hammer-Aitoff full-sky composite projection from 2 February 2003 created from around 4500 individual SMEI camera image frames [*Jackson et al.*, 2004]. This is a typical SMEI sky map from a single orbit around the Earth.

Coles, 1972]. The time lag for which maximum cross correlation occurs (taking into account ''plane-of-sky'' assumptions) can then be used to estimate the outflow speed of the irregularities producing the scintillation. More sophisticated methods include fitting a weak-scattering model to the observed autocorrelation and cross-correlation spectra [e.g., *Coles*, 1996; *Klinglesmith*, 1997; *Bisi et al.*, 2007; *Breen et al.*, 2008].

[4] SMEI was launched on 6 January 2003 into a Sun-synchronous polar orbit aboard the US Air Force Space Test Program, the Coriolis satellite. Conceived as an all-sky imager [*Jackson et al.*, 1989], SMEI views the outward flow of structures in the solar wind using three cameras, by observing Thomson-scattered white light from electrons in the heliospheric plasma (Figure 1). Each baffled camera has a 60° field of view, the ensemble provides a 160° of sky coverage with a 20° exclusion zone toward the Sun. Approximately 1500 four-second exposures from each of the cameras (approximately 4500 in total) are combined to create a near-all-sky map with an orbital cadence of

Table 1. Summary of the Events Investigated Here in Chronological Order of Their Possible Source(s) as Seen by the SOHO|LASCO C2 Instrument[a]

Possible LASCO C2 Source (CME)	Interplanetary Counterpart First Seen at ACE	Geomagnetic Activity (*Dst* Minimum)
4 Nov 2004 – 0954 UT Halo	7 Nov 2004 – 2230 UT	8 Nov 2004 – 0700 UT
4 Nov 2004 – 2330 UT Partial Halo	7 Nov 2004 – 2230 UT	8 Nov 2004 – 0700 UT
6 Nov 2004 – 0132 UT Halo	9 Nov 2004 – 2025 UT	10 Nov 2004 – 1000 UT
6 Nov 2004 – 0206 UT Partial Halo	9 Nov 2004 – 2025 UT	10 Nov 2004 – 1000 UT
7 Nov 2004 – 1654 UT Halo	9 Nov 2004 – 2025 UT	10 Nov 2004 – 1000 UT

[a]Information partially taken from *Zhang et al.* [2007] and also from *Harra et al.* [2007].

102 minutes. The structures which SMEI observes include coronal mass ejections (CMEs), corotating structures (interaction regions), and other density enhancements or depletions in solar wind outflow. SMEI may be regarded as a successor to the zodiacal light photometers [*Leinert et al.*, 1975] on the two Helios spacecraft, building on the heliospheric remote-sensing capabilities that were demonstrated by the Helios photometers [e.g., *Jackson*, 1985]. The SMEI instrument design, architecture, testing, and qualification procedures, are described by *Eyles et al.* [2003], and the history of the SMEI design and development, including a description of the mission, data handling, and removal of background sources during image processing, are given by *Jackson et al.* [2004], *Hick et al.* [2005, 2007], and *Buffington et al.* [2006a, 2006b, 2007].

[5] We use a purely kinematic solar wind model to yield three-dimensional (3-D) speed and density tomographic reconstructions [*Hick and Jackson*, 2004]. The technique obtains perspective views of outward flowing solar wind [*Jackson and Hick*, 2005] crossing lines of sight from Earth to the radio sources, by iteratively fitting the model to the IPS data. We also use the output of these tomographic reconstructions to provide a ''source surface'' input into the ENLIL 3-D magnetohydrodynamic (MHD) numerical model [e.g., *Odstrcil and Pizzo*, 2002] which is then propagated out through the interplanetary medium. We then compare the resulting 3-D reconstructions and MHD modeling with near-Earth in situ measurements.

[6] We first briefly describe this October/November 2004 observation period in section 2. Section 3 deals with the IPS and SMEI analyses [e.g., *Jackson and Hick*, 2005] including our 3-D tomographic reconstructions. Further details regarding the full SMEI analyses carried out here are given by *Jackson et al.* [2008], and a comparison with the ENLIL 3-D MHD numerical model is given by *Odstrcil and Pizzo* [2002]. Section 4 discusses the results. Concluding remarks follow in section 5.

2. Observation Period

[7] October/November 2004 was a time of complex activity with multiple CME features (including several ''Halo'' and ''Partial Halo'' CMEs) seen in coronagraph images and the interplanetary counterparts (ICMEs) measured by spaceborne in situ plasma and magnetic-field instruments near Earth. The period investigated here included several ICMEs arising from a series of solar eruptions (including flares, transequatorial loops and filaments, and coronal hole interactions) originating from the Sun between 4 November 2004 and 8 November 2004 (discussed in detail by *Harra et al.* [2007]). During this period, two ICMEs with magnetic cloud (MC) characteristics occurred which had opposing magnetic orientations despite the fact that they were related to flares coming from above the same active region (AR) on the Sun. During these eruptions, the AR's magnetic configuration remained unchanged throughout [*Harra et al.*, 2007]. A subset of ICMEs can be classified as MCs as is done here. This special case of ICME was defined by *Burlaga* [1995] as having strong magnetic fields (when compared with the surroundings) displaying a large and coherent rotation, and depressed ion temperature; these thus were named as MCs.

[8] The Living With a Star (LWS) Coordinated Data Analysis Workshop (CDAW) study conducted by *Zhang et al.* [2007] also included these early November 2004 events during their extensive analyses of large geoeffective storms with *Dst* (disturbance storm time index) ≤ -100 nT storms occurring between 1996 and 2005. They list two possible CME sources for each of the two large storms, and *Harra et al.* [2007] also include a third CME possible source for the second of the two geomagnetic storms. The first storm's *Dst* minimum occurred on 8 November 2004 at 0700 UT and the second on 10 November 2004 at 1000 UT. The possible sources for the first storm as seen by the SOlar and Heliospheric Observatory - Large Angle Spectrometric COronagraph (SOHO|LASCO) [*Domingo et al.*, 1995; *Brueckner et al.*, 1995] C2 instrument on 4 November 2004 at 2330 UT and at 0954 UT. The second storm's possible sources occurred on 7 November 2004 at 1654 UT and 6 November 2004 at 0206 UT, with the third from *Harra et al.* [2007] being 6 November 2004 at 0132 UT. These two geomagnetic storms were related to the two ICME MCs measured in situ and the first detection of these at L_1 were on 7 November 2004 at 2230 UT for the first geomagnetic storm, and on 9 November 2004 at 2025 UT for the second geomagnetic storm (i.e., the first MC created the first geomagnetic storm, and the second MC created the second geomagnetic storm). Also, out of the two major geomagnetic storms that hit the Earth, the first was predominantly related to AR10696, and the other was either from an erupting transequatorial filament, or else a rotation of 160° of a flux rope in the same AR [*Harra et al.*, 2007]. In total for this time period, there were five CMEs (three halo and two partial halo), two ICMEs identified as MCs, and two geomagnetic storms at the Earth with *Dst* ≤ -100 nT.

[9] Table 1 gives an overview of the source regions (CMEs), interplanetary signatures (ICMEs/MCs), and geomagnetic storms during this period about which this paper is

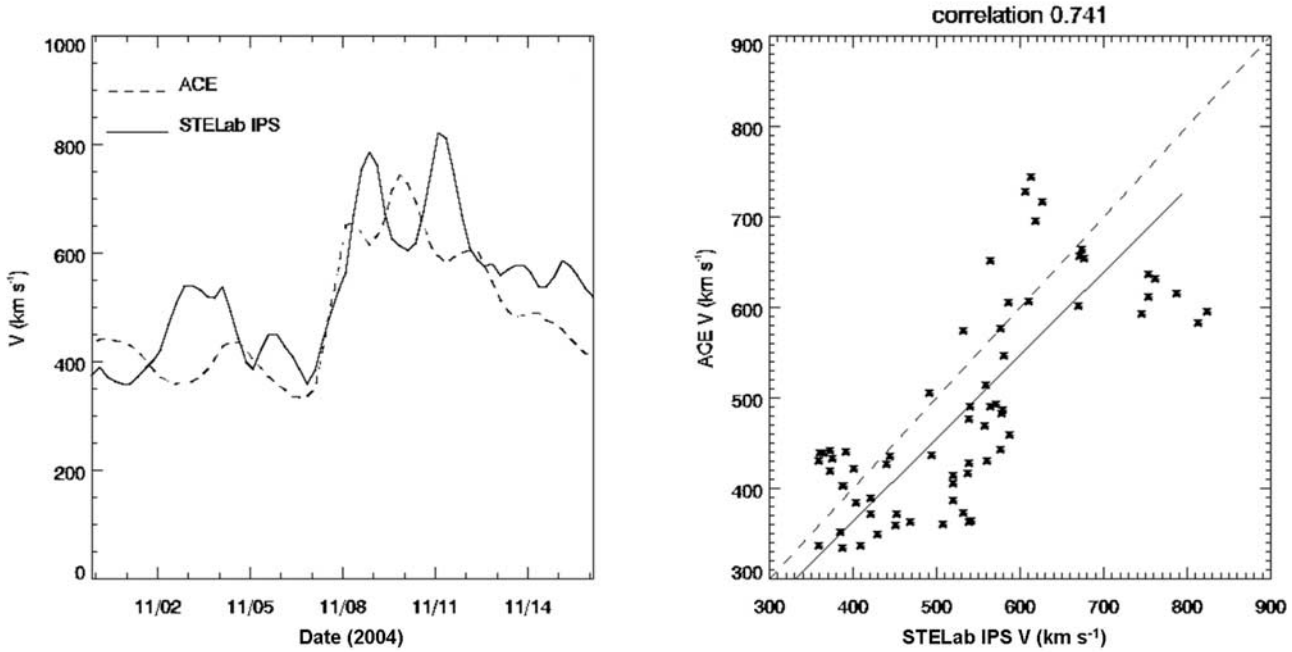

Figure 2. The left plot shows a comparison of solar wind speed reconstructed at ACE using the IPS observations from STELab (solid line), and those actually measured by ACE (Level 0 data), located at the L_1-point ~1% toward the Sun from Earth (dashed line). The ACE data are hourly averaged data that have been further averaged with a daily cadence to match that of the IPS reconstruction. On the right is a plot of the correlation of the two data sets, the dashed line for a 100% correlation and the solid line the best fit of the correlation. A similar picture is seen when comparing with Wind in situ plasma data. A more complete description of the data is found in the text.

concerned, and provides a brief overview of their interconnecting relationships.

3. Observations and Analyses

[10] Both the STELab 327 MHz IPS observations and SMEI white light data are analyzed using a 3-D time-dependent kinematic model [*Jackson and Hick*, 2005; *Jackson et al.*, 2006; Jackson et al., submitted manuscript, 2008]. The SMEI data are also analyzed using the ENLIL 3-D MHD numerical model [e.g., *Odstrcil and Pizzo*, 1999, 2002].

3.1. IPS Observations and Speed Reconstructions Using a 3-D Kinematic Model

[11] Radio sources beyond 11.5° solar elongation (typically to ~60° at 327 MHz, depending on the availability and strength of radio sources) were used in the speed reconstructions for the tomographic kinematic model. IPS observations throughout this period cover sources mainly in the northern half of the heliosphere because of STELab's northern location on the Earth and the Sun's southern position at this time of year. Thus here, the IPS observations are useful only to reconstruct heliospheric structure in the northern hemisphere and through to just south of the ecliptic. Any reconstruction farther south would be considered suspect because of there being so few data points to reconstruct from. The digital resolution of the IPS reconstruction, where possible along the heliographic equator and in the northern hemisphere, is limited to 20° latitude and longitude spatial resolution and a temporal cadence of 1 day [see *Jackson and Hick*, 2005]. At this resolution, the reconstructed speed compares well with ACE in situ L_1 observations (also averaged over a 1-day cadence) when using both the IPS speed, and its scintillation level converted to g level value as a proxy for density (see Figure 2).

[12] As described in detail by *Jackson and Hick* [2005] and taken from *Bisi et al.* [2008], scintillation level measurements have been available from STELab since 1997. The disturbance factor g is defined by equation (1).

$$g = m/\langle m \rangle \tag{1}$$

[13] In relation to equation (1), $\Delta I/I$ is the ratio of source intensity variation to measured signal intensity; m is the observed fractional scintillation level; and $\langle m \rangle$ is the modeled mean level of $\Delta I/I$ for the source at its elongation and gain calibration at the time of its observation. Scintillation level measurements from STELab analyses are available at a given sky location as an intensity variation of the source signal strength. For each of the sources, data are automatically edited to remove any obvious interference discerned in the daily STELab observations. Further discussion regarding the calculation of and the use of g level as a proxy for density is provided by *Hick and Jackson* [2004] and *Jackson and Hick* [2005].

[14] Figure 3 (adapted from *Harra et al.* [2007]) is an IPS 3-D reconstruction of speed using the same analysis as for Figure 2. The image shows the high-speed Earth-directed CME events (that were also seen by LASCO C2 on

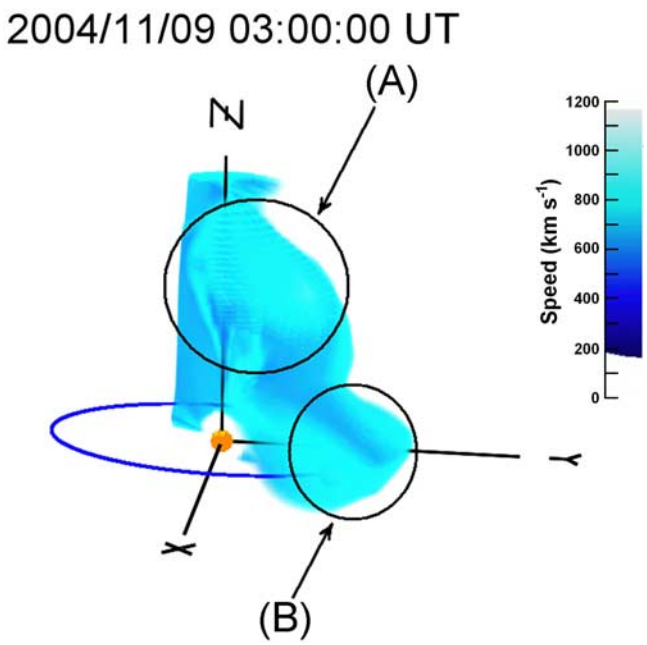

Figure 3. A 3-D tomographic reconstruction of solar wind speed as viewed by a remote observer looking from east of the Sun-Earth line and ~15° above the ecliptic plane (adapted from *Harra et al.* [2007] with permission from Springer Science + Business Media). The IPS data are reconstructed here, for the time shown, out to a distance of 1.5 AU from the Sun. The scaling of the speed is determined by the brightness of the image; the darker the color, the lower the value for speed in a range starting at 900 km s^{-1} and upward thereof (and also seen by the colored bar alongside the image). Everything in the southern hemisphere, in the foreground, and opposite the Sun from the Earth has been removed for ease of viewing and to limit obscuration of the points of interest in this reconstructed image. The Earth is engulfed inside the high-speed structure in the ecliptic. Features A and B are explained in section 4.

6 November 2004 and 7 November 2004), to the northwest of the Sun-Earth line at 0300 UT on 9 November 2004.

3.2. SMEI Observations and Density Reconstructions Using a 3-D Kinematic Model

[15] As described in section 2, the heliosphere was complex at this time with many interplanetary events detected in situ. Figure 4 presents a summary comparison of reconstructed SMEI density compared with ACE and Wind in situ measurements. SMEI reconstructions are currently limited by computer analysis considerations and have in general ~3 times finer resolution than the IPS reconstructions. This latter results from the more numerous available lines of sight, since SMEI does not require bright astronomical radio sources in the sky as does IPS.

[16] To compare with in situ proton density measurements, the present analysis includes an electron excess due to helium and heavier ions, and conversion of SMEI surface brightness units of 0.46 ± 0.02 ADU = one S10 [*Buffington et al.*, 2007]. An S10 is the intensity of a 10th magnitude star spread over one square degree of the sky [see *Jackson et al.*, 2006], and an ADU is the SMEI Analog-to-Digital Unit. IPS speed data were incorporated to improve the global distribution of SMEI density structures in the SMEI reconstructions. These SMEI reconstructions have a digital resolution of 6.7° by 6.7° in latitude and longitude at a 1/2-day temporal cadence, and use measurements along ~200,000 lines of sight taken from star-subtracted maps (as described by *Hick et al.* [2007] and *Jackson et al.* [2008]). Ultimately, the lines of sight could in principle number into the tens of millions if the quality of data is sufficient and the computational resources are available to process a model resolution that can then take advantage of the high line-of-sight count.

[17] SMEI observations cover nearly the entire sky, ranging from ~20° elongation in camera 3 to ~180° elongation in camera 1. The 2-D cuts through the 3-D reconstructed volumes (Figure 5) for the SMEI analyses remain blank where there are too few lines of sight to provide 3-D reconstructions at the resolution mentioned earlier; this includes the region opposite Earth on the far side of the Sun. The 3-D reconstruction can also sometimes produce noise along the cutoff boundary.

[18] From a finalized calibration from ADUs to S10s and to match the proton number measurements observed in situ by spacecraft, we assume an electron excess of 20% from ionized helium and heavy ions, thus resulting in a conversion factor from SMEI ADUs to S10 Units of 0.552 ADU per S10. This calibration depends somewhat on the helium-to-hydrogen ratio (He/H) which can vary somewhat for different solar wind structures. To first order, the SMEI 3-D reconstructions shown scale linearly with this calibration factor. Further details are given by *Jackson et al.* [2008].

[19] Figure 5 shows cuts through the reconstructed density volume in the ecliptic plane looking from the north and also in the meridional plane as if looking from east of the Sun-Earth line out to 1.5 AU. Figure 5 shows the shape of the density reconstruction as extracted from the 3-D tomography at 0000 UT of the days of the two CDAW storms impacting upon the Earth.

3.3. SMEI Density Reconstructions Using the ENLIL 3-D MHD Model

[20] The ENLIL numerical model is an MHD code for simulating the background solar wind and solar transients (such as CMEs and shocks) in the inner heliosphere and midheliosphere regions. The model is based on ideal MHD equations; the ratio of specific heats, γ, is usually chosen to be 1.5. The explicit finite-difference-modified high-resolution Total-Variation-Diminishing Lax-Friedrich (TVDLF) scheme [*Tóth and Odstrcil*, 1996, and references therein] is used on a fixed uniform (or nonuniform, which is used for pole-to-pole computations) numerical grid. Large variations in the solar wind plasma properties between the Sun and the Earth leads to different physical processes and phenomena in different spatial domains. We interface between inner coronal regions and heliospheric regions by using an inner boundary region, in this case located at 35 $R_\odot$ from the center of the Sun. We employ our time-dependent 3-D solar wind tomographic results of plasma density and flow velocity at 35 $R_\odot$ to use as a source surface of boundary conditions for the MHD model. Temperature is

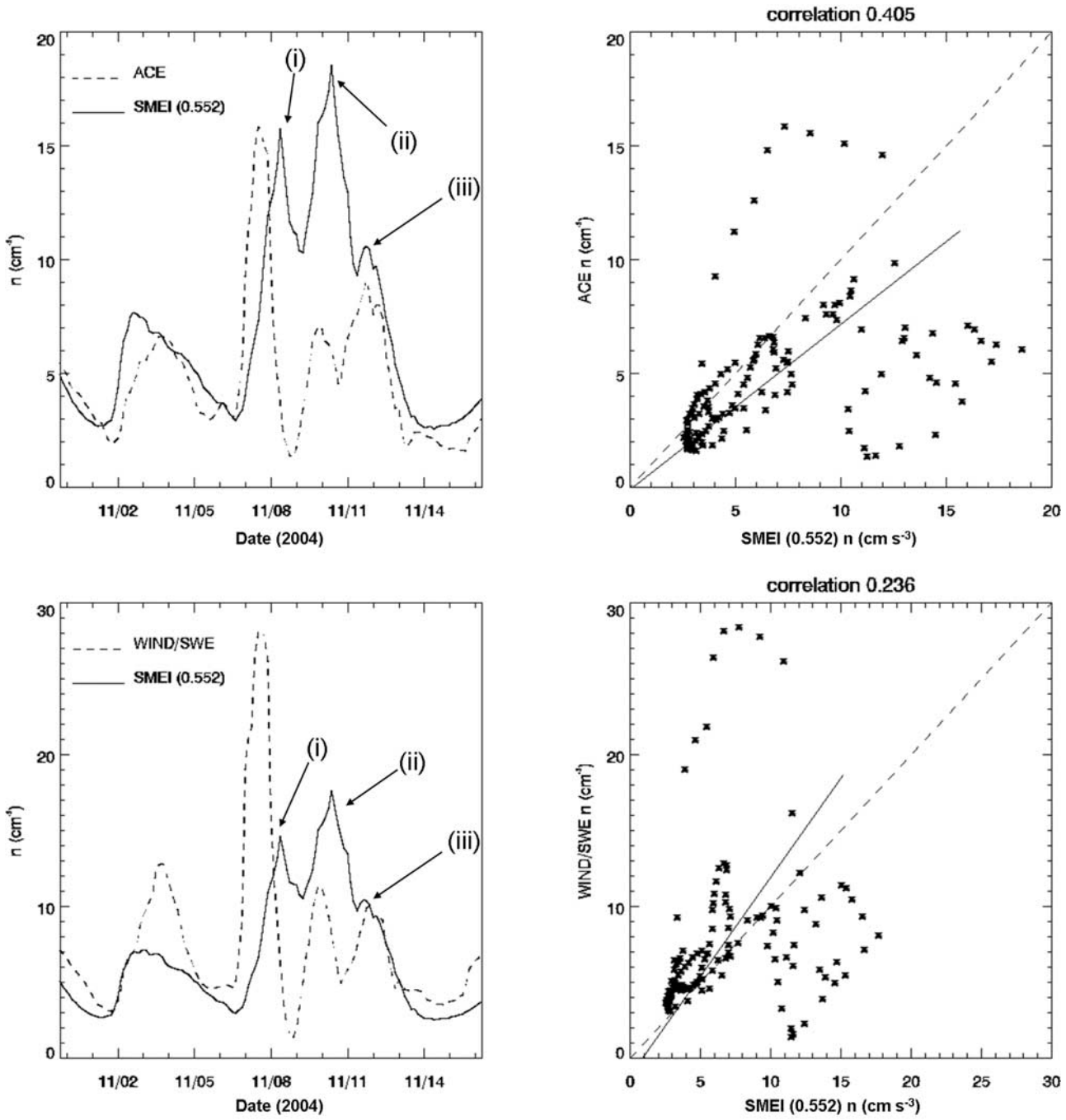

Figure 4. The top left plot compares the density reconstructed at ACE using SMEI Thomson-scattered white light observations (solid line) with ACE measurements (dashed line), and similarly for the bottom left plot for Wind plasma data. Both the ACE and Wind data are hourly averaged data that have again been further averaged with a daily cadence. The top right plot shows the correlation of the two data sets for ACE and similarly the bottom right for Wind; the dashed line on each correlation plot for a 100% correlation and the solid line the best fit of the data here. Features i, ii, and iii on the left-hand plots relate to features highlighted in Figure 5 and also described in section 4.

not of significant importance in the dynamics in the heliosphere above 35 $R_\odot$ and is derived from balancing the total pressure; the magnetic field input can be used from other coronal models. Further details are given by *Odstrcil and Pizzo* [1999, 2002].

[21] Figure 7 shows the simulation results for 08 November 2004 roughly matching those shown in Figure 5 for ecliptic and meridional cuts through the 3-D simulation, and also Figure 4 for in situ comparisons with ACE data. Global

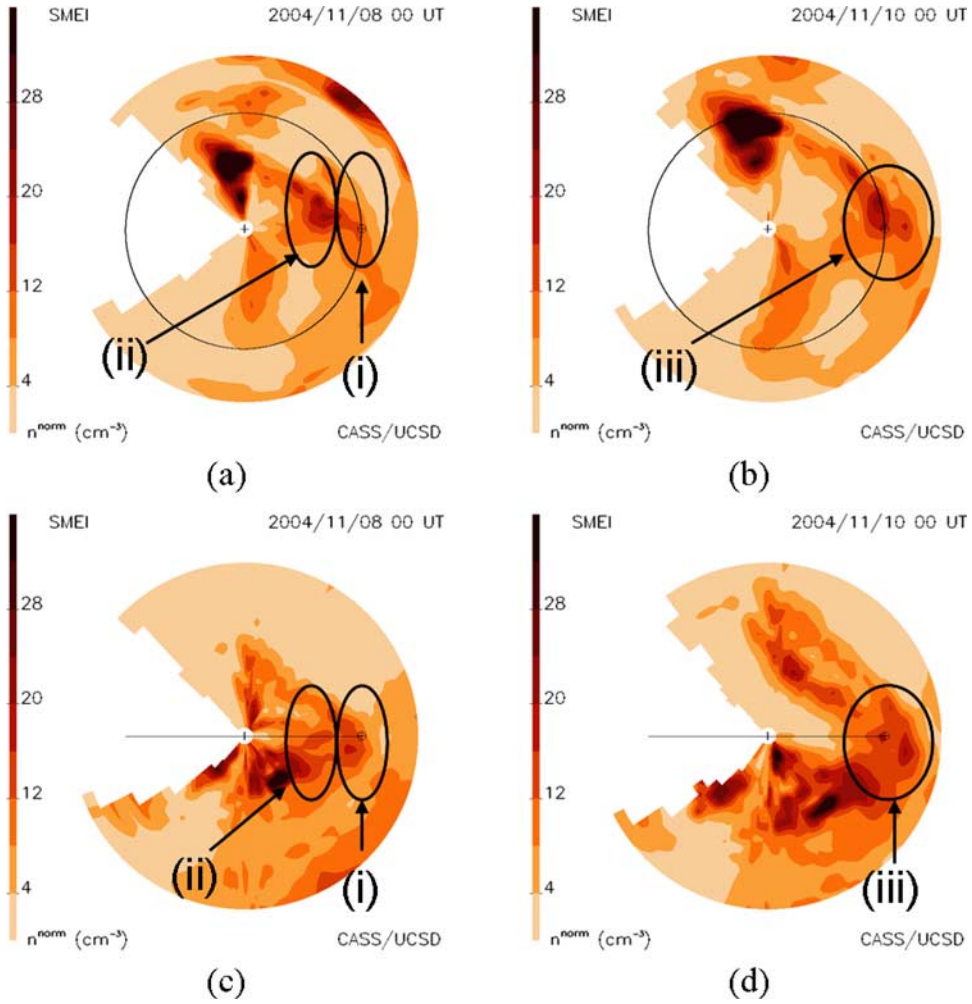

Figure 5. Summary of low-resolution (a and b) ecliptic and (c and d) meridional cuts through the SMEI 3-D density reconstructions out to 1.5 AU at the times shown. Various features are circled in the images which are also labeled in Figure 4 and discussed in section 4. Earth's orbit is shown as a circle or line with the Earth, $\oplus$, indicated on each plot. The expected r^{-2} density falloff scaling is used to normalize structures at different radii. Density contours to the left of each image are scaled to 1 AU.

and ICME structure in the ENLIL 3-D simulation are similar to the SMEI 3-D tomographic reconstruction.

4. Discussion

[22] The LWS CDAW storms [*Zhang et al.*, 2007] reached *Dst* minima on 8 and 10 November 2004 at 0700 UT and 1000 UT, respectively. The interplanetary drivers of these storms are 3-D reconstructed (as seen in Figures 3 and 5) and show what could be described as a "combining or amalgamating of events" in the inner heliosphere, which then led to the large geoeffective space weather storms seen at Earth. What the "combining" seen in the reconstruction means is presently difficult to understand; it may be the interaction of CMEs to form the interplanetary counterparts, or simply that the CMEs seen separately in white light coronagraph data catch up with previous CMEs and merge somewhere between the Sun and the Earth.

[23] Figure 3 shows that major structures observed to the north have been reconstructed in velocity, and are evaluated near Earth where they can also be measured in situ. The resolution of the reconstructions allows us to distinguish the components of individual CMEs, components which could not have been otherwise separated in the data. The reconstructions show (feature A) a high-speed structure going mainly northward and (feature B) a high-speed structure engulfing the Earth which lags the 6 November 2004 Earth-directed events (0132 UT halo CME and 0206 UT partial halo CME) but precedes the 7 November 2004 event. Its determined speed is comparable to that detected by LASCO C2 for the 7 November 2004 1654 UT halo CME. This is also discussed by *Harra et al.* [2007]. The high-speed structure going mainly northward (feature A) is most likely related to at least one of the many CMEs during this time period but not necessarily any of the five discussed here.

[24] SMEI density analyses, Figures 4 and 5, have a finer digital resolution (6.7° by 6.7°) of the individual structures of this complex set of events than the IPS speed reconstructions (20° by 20°). Figure 4 shows that the overall increase in density associated with these events measured in situ from 7 to 12 November 2004 is reconstructed fairly accurately (at least in time if not in magnitude). Individual

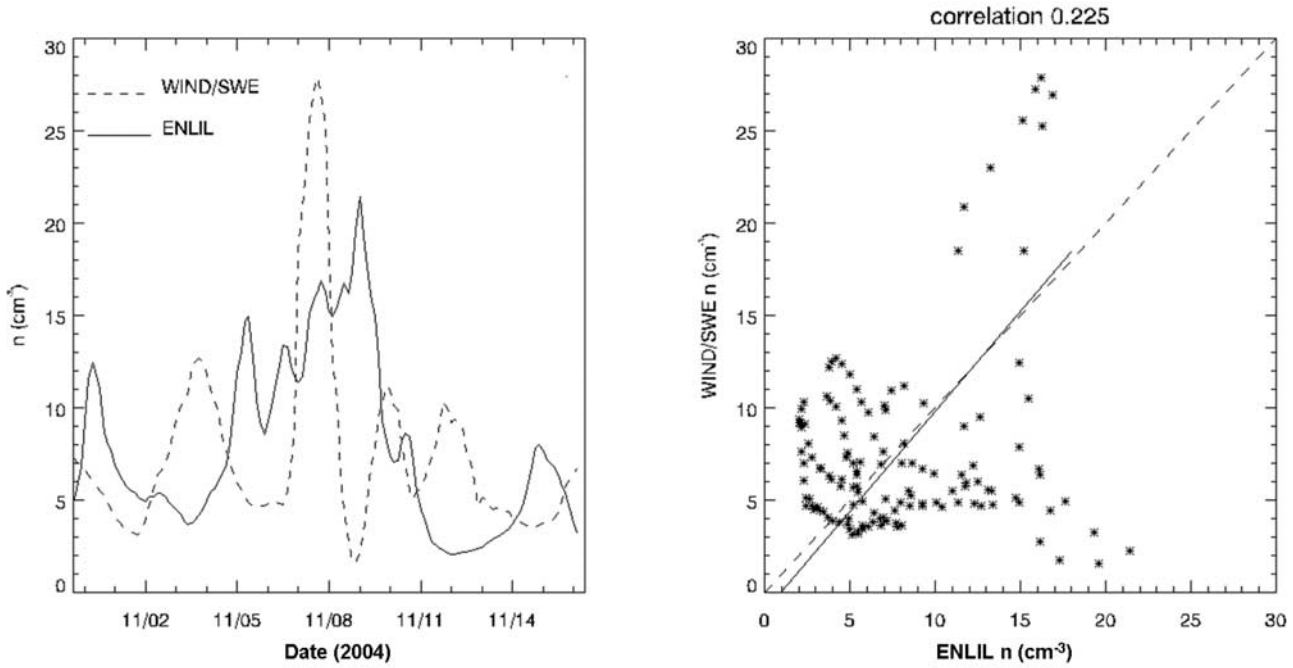

Figure 6. A summary of the ENLIL 3-D numerical model results for in situ comparison with Wind hourly averaged proton density data (further averaged to a daily cadence) and corresponding correlation plot (as in the bottom plot of Figure 4).

density peaks measured by ACE (and Wind) on 7, 10, and 12 November 2004, are also matched well in the 3-D model reconstructions near Earth. Figure 5 shows the 3-D structure of the events consistent with peaks in density measured by ACE and Wind, and which are associated with the halo CME event sequences observed by LASCO during this period. Various density features are highlighted in Figures 4 and 5: Feature i is a heliospheric structure associated with the front edge of the interplanetary disturbance which caused the 8 November 2004 geomagnetic storm, most likely caused by a combination of Earth-directed CMEs seen in LASCO on 4 November 2004 at 0954 UT and 2330 UT; feature ii is a combination of the 6 November 2004, 0132 UT (halo) and 0206 UT, LASCO C2 CMEs, consistent with the STELab IPS density reconstruction shown by *Harra et al.* [2007]; and feature iii is a heliospheric structure during the second of the two CDAW storms beginning on 10 November 2004. The reconstruction in Figures 5b and 5d shows what seems to be a combination of the previous events seen in feature ii but at the later time; and most likely some kind of amalgamation with the faster 7 November 2004 at 1654 UT (halo) event as they pass Earth. These are again consistent with the findings of *Harra et al.* [2007] and *Zhang et al.* [2007].

[25] Present University of California, San Diego (UCSD) 3-D reconstructions incorporate a kinematic model, and merging/interaction between events of differing speeds are probably not accurately reproduced at the resolutions available in the present work. Although individual density peaks measured by ACE are reproduced in the middle of the SMEI density reconstructed period from around 10 November 2004, the base from which these peaks arise does not match as well (at least from the comparison with the ACE data). A structure to the north in the 3-D reconstructions shown in Figure 5 is located in the same general vicinity as the high-speed structure reconstructed from the IPS observations seen in Figure 3. However, this structure is suspicious because it is so dense and since there are no in situ measurements at that location, we cannot ascertain if it is real.

[26] Figure 6 shows an in situ plot (as in the bottom plot of Figure 4), and Figure 7 shows meridional and ecliptic cuts (as in Figure 5). These are using the reconstructed results obtained from the ENLIL numerical model that uses the kinematic model inner boundary as input. As can be seen, the features in the ecliptic and meridional cuts are similar to those seen in Figure 5 but perhaps marginally earlier in their arrival time; and also there is a good comparison, possibly better even, with Wind data, than that seen in Figure 4, despite the actual correlation value with the Wind data being slightly smaller. However, there is still a discrepancy in terms of the drops in density between each of the peaks which is also seen in the kinematic model only, as well as here using the MHD numerical code. Overall however, the match in density here seems to be improved through the use of the ENLIL model for the first of the two magnetic clouds at least. A plausible reason for the drops not being as great in magnitude as those recorded in situ is simply that the present model resolution is insufficient to detect such large drops in density between the peaks.

5. Conclusions

[27] The interplanetary drivers of these LWS CDAW storms are fairly well reproduced both in IPS speed and SMEI density 3-D reconstructions (using both forms of the model) and are consistent with CME events seen in LASCO

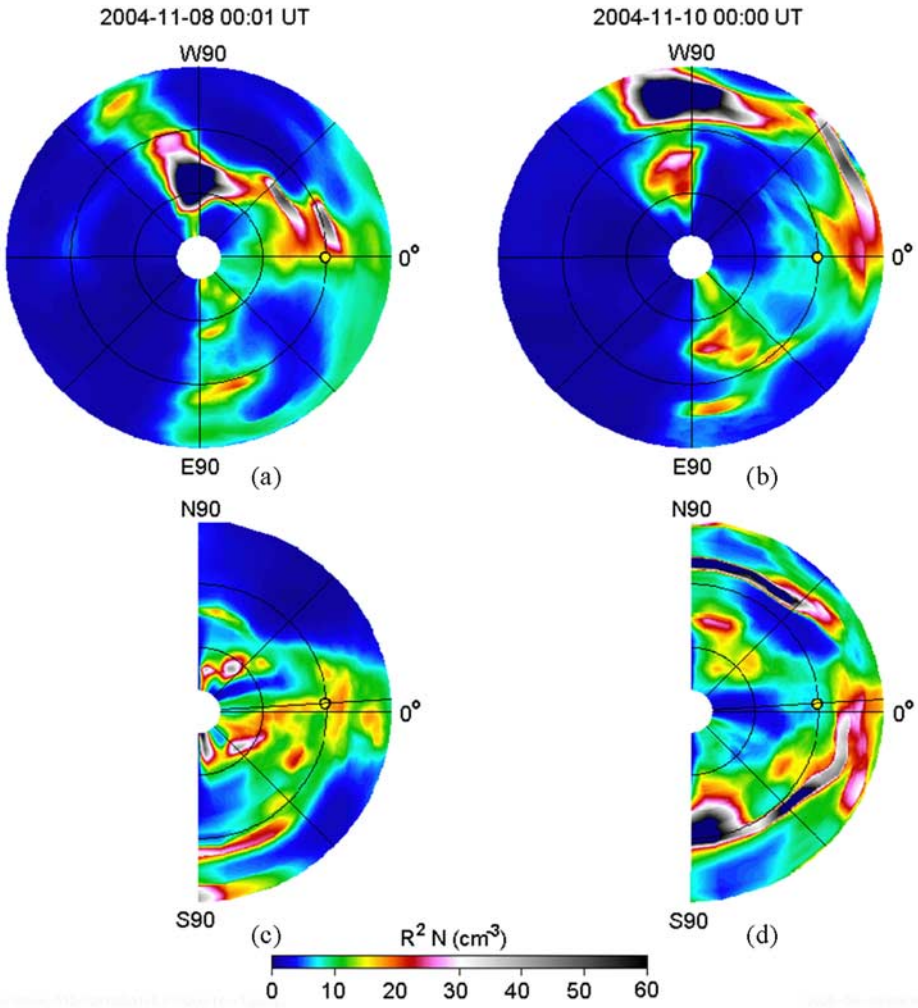

Figure 7. A summary of the ENLIL 3-D numerical model results for 8 November 2004 and 10 November 2004 at midnight UT as (a and b) ecliptic and (c and d) meridional cuts (as in Figure 5).

and associated with known interplanetary in situ signatures. The IPS data show the fast CME speeds seen in LASCO heading to the north and northwest as well as those engulfing Earth during the same time period as detected in situ at ACE. The structures reproduced around Earth from SMEI data show a combination of several Earth-directed/near-Earth-directed events in density. These structures seen in SMEI are consistent with the timing of the geoeffective storms during this period where the two *Dst* minima occurred on 8 November 2004 at 0700 UT and 10 November 2004 at 1000 UT. The larger differences measured in situ not being well matched by the reconstructed data could be due to two possible reasons: the kinematic model not dealing well with shocks, or the low-resolution reconstructions being insufficient to effectively resolve the large, short-time-scale differences between the peaks (and thus between events or parts of events).

[28] We have merged the UCSD 3-D kinematic model results at 35 $R_\odot$ with the ENLIL 3-D simulation. Upon running the MHD code with the input from the kinematic model as an inner boundary, the results of CME development through the inner heliosphere are similar to those seen from the 3-D UCSD kinematic tomographic model. This is an encouraging result for further case studies and the eventual inclusion of an MHD code into the UCSD 3-D tomography thus replacing the present kinematic solar wind model.

[29] We expect that these reconstructions can be improved by employing greater numbers of lines of sight and the higher resolution that results from these data sets. Alternative solar wind models that can better handle interactions from multiple successive events and take account of shocks may also potentially yield better 3-D reconstructions, such as the full incorporation of MHD numerical code.

[30] We look forward to multipoint in situ comparisons from the Solar TErrestrial Relations Observatory (STEREO) [*Kaiser*, 2005] and from Ulysses [*Wenzel et al.*, 1992] spacecraft that will improve the 3-D reconstructions by providing additional heliospheric locations for which to calibrate and adjust our solar wind model.

[31] **Acknowledgments.** The authors acknowledge AFOSR grant FA9550-06-1-0107, NSF grant FA8718-04-C-0050, and NASA grant NNG05GM58G for support to work on these analyses. The authors acknowledge and thank the group at STELab, Nagoya University, Japan (M. Kojima, M. Tokumaru, K. Fujiki, and students), for their continued

support and for making the IPS data available under the auspices of a joint collaborative agreement between the Center for Astrophysics and Space Sciences, University of California at San Diego, and STELab. SMEI was designed and constructed by a team of scientists and engineers from the U.S. Air Force Research Laboratory, the University of California at San Diego, Boston College, Boston University, and the University of Birmingham, UK. The authors also wish to thank the ACE|SWEPAM and Wind|SWE groups for use of their data.

[32] Amitava Bhattacharjee thanks Michael Kaiser and another reviewer for their assisstance in evaluating this paper.

References

Armstrong, J. W., and W. A. Coles (1972), Analysis of three-station interplanetary scintillation data, *J. Geophys. Res.*, *77*, 4602.

Bisi, M. M., A. R. Breen, R. A. Fallows, P. Thomasson, R. A. Jones, and G. Wannberg (2005), Combined EISCAT/ESR/MERLIN interplanetary scintillation observations of the solar wind, in *"Connecting Sun and Heliosphere": Proceedings of Solar Wind 11/SOHO 16*, edited by B. Fleck and T. H. Zurbuchen, *Eur. Space Agency Spec. Publ.*, ESA-SP 592, 593-596.

Bisi, M. M., R. A. Fallows, A. R. Breen, S. Rifai Habbal, and R. A. Jones (2007), Large-scale structure of the fast solar wind, *J. Geophys. Res.*, *112*, A06101, doi:10.1029/2006JA012166.

Bisi, M. M., B. V. Jackson, P. P. Hick, A. Buffington, and J. M. Clover (2008), Coronal mass ejection reconstructions from interplanetary scintillation data using a kinematic model: A brief review, in *Proceedings of the AOGS 2007 Meeting: Advances in Geosciences*, in press.

Breen, A. R., R. A. Fallows, M. M. Bisi, R. A. Jones, B. V. Jackson, M. Kojima, G. D. Dorrian, H. R. Middleton, P. Thomasson, and G. Wannberg (2008), The solar eruption of 2005 May 13 and its effects: Long-baseline interplanetary scintillation observations of the Earth-directed coronal mass ejection, *Astrophys. J. Lett.*, *683*, L79–L82, doi:10.1086/591520.

Brueckner, G. E., et al. (1995), The Large Angle Spectroscopic Coronagraph (LASCO), *Sol. Phys.*, *162*, 357–402.

Buffington, A., D. L. Band, B. V. Jackson, P. P. Hick, and A. C. Smith (2006a), A search for early optical emission at gamma-ray burst locations by the Solar Mass Ejection Imager (SMEI), *Astrophys. J.*, *637*, 880–888, doi:10.1086/498407.

Buffington, A., B. V. Jackson, P. Hick, and S. D. Price (2006b), An empirical description of zodiacal light as measured by SMEI, *Eos Trans. AGU*, *87*(52), Fall Meeting Suppl., Abstract SH32A-06.

Buffington, A., J. S. Morrill, P. P. Hick, R. A. Howard, B. V. Jackson, and D. F. Webb (2007), Analysis of the comparative responses of SMEI and LASCO, *Proc. SPIE*, *6689*, 66890B, doi:10.1117/12.734658.

Burlaga, L. F. (1995), *Interplanetary Magnetohydrodynamics*, Oxford Univ. Press, New York.

Coles, W. A. (1996), A bimodal model of the solar wind speed, *Astrophys. Space Sci.*, *243*(1), 87–96.

Coles, W. A., and S. Maagoe (1972), Solar wind velocity from IPS observations, *J. Geophys. Res.*, *77*, 5622–5624.

Domingo, V., B. Fleck, and A. I. Poland (1995), SOHO: The Solar and Heliospheric Observatory, *Space Sci. Rev.*, *72*, 81.

Eyles, C. J., G. M. Simnett, M. P. Cooke, B. V. Jackson, A. Buffington, P. P. Hick, N. R. Waltham, J. M. King, P. A. Anderson, and P. E. Holladay (2003), The Solar Mass Ejection Imager (SMEI), *Sol. Phys.*, *217*, 319–347.

Fallows, R. A., P. J. S. Williams, and A. R. Breen (2002), EISCAT measurements of solar wind velocity and the associated level of interplanetary scintillation, *Ann. Geophys.*, *20*, 1279.

Fallows, R. A., A. R. Breen, M. M. Bisi, R. A. Jones, and G. Wannberg (2006), Dual-frequency interplanetary scintillation observations of the solar wind, *Geophys. Res. Lett.*, *33*, L11106, doi:10.1029/2006GL025804.

Harra, L. K., N. U. Crooker, C. H. Mandrini, L. van Driel-Gesztelyi, S. Dasso, J. Wang, H. Elliott, G. Attrill, B. V. Jackson, and M. M. Bisi (2007), How does large flaring activity from the same active region produce oppositely directed magnetic clouds?, *Sol. Phys.*, *244*, 95–114, doi:10.1007/s11207-007-9002-x.

Hewish, A., P. F. Scott, and D. Wills (1964), Interplanetary scintillations of small diameter radio sources, *Nature*, *203*, 1214.

Hick, P., A. Buffington, and B. V. Jackson (2005), The SMEI real-time data pipeline: From raw CCD frames to photometrically accurate full-sky maps, in *Solar Physics and Space Weather Instrumentation*, edited by S. Fineschi and R. A. Viereck, *Proc. SPIE*, *5901*, 340–346, doi:10.1117/12.617996.

Hick, P. P., and B. V. Jackson (2004), Heliospheric tomography: An algorithm for the reconstruction of the 3D solar wind from remote sensing observations, in *Telescopes and Instrumentation for Solar Astrophysics*, edited by S. Fineschi and M. A. Gummin *Proc. SPIE*, 5171, 287–297, doi:10.1117/12.513122.

Hick, P. P., A. Buffington, and B. V. Jackson (2007), A procedure for fitting point sources in SMEI white-light full-sky maps, *Proc. SPIE*, *6689*, 66890C, doi:10.1117/12.734808.

Jackson, B. V. (1985), Imaging of coronal mass ejections by the HELIOS spacecraft, *Sol. Phys.*, *100*, 563–574.

Jackson, B. V., and P. P. Hick (2005), Three-dimensional tomography of interplanetary disturbances, in *Solar and Space Weather Radiophysics: Current Status and Future Developments*, *Astrophys. Space Sci. Libr.*, vol. 314, edited by D. Gary and C. U. Keller, chap. 17, pp. 355–386, Kluwer Acad., Dordrecht, Netherlands.

Jackson, B. V., H. S. Hudson, J. D. Nichols, and R. E. Gold (1989), Design considerations for a "solar mass ejection imager" on a rotating spacecraft, in *Solar System Plasma Physics*, *Geophys. Monogr. Ser.*, vol. 54, edited by J. H. Waite Jr., J. L. Burch, R. L. Moore, p. 291, AGU, Washington, D. C.

Jackson, B. V., et al. (2004), The Solar Mass Ejection Imager (SMEI) mission, *Sol. Phys.*, *225*, 177–207, doi:10.1007/s11207-004-2766-3.

Jackson, B. V., A. Buffington, P. P. Hick, X. Wang, and D. Webb (2006), Preliminary three-dimensional analysis of the heliospheric response to the 28 October 2003 CME using SMEI white-light observations, *J. Geophys. Res.*, *111*, A04S91, doi:10.1029/2004JA010942.

Jackson, B. V., M. Bisi, P. Hick, A. Buffington, J. Clover, and W. Sun (2008), Solar Mass Ejection Imager 3-D Reconstruction of the 27–28 May 2003 CME sequence, *J. Geophys. Res.*, doi:10.1029/2008JA013224, in press.

Kaiser, M. L. (2005), The STEREO mission: An overview, *Adv. Space Res.*, *36*, 1483–1488.

Klinglesmith, M. (1997), The polar solar wind from 2.5 to 40 solar radii: Results of intensity scintillation measurements, Ph.D. thesis, Univ. of Calif., San Diego.

Kojima, M., and T. Kakinuma (1987), Solar cycle evolution of solar wind speed structure between 1973 and 1985 observed with the interplanetary scintillation method, *J. Geophys. Res.*, *92*, 7269–7279.

Leinert, C., H. Link, E. Pitz, N. Salm, and D. Knüppelberg (1975), The Helios zodiacal light experiment (E9), *Raumfahrtforschung*, *19*, 264–267.

McComas, D. J., S. J. Bame, P. Barker, W. C. Feldman, J. L. Phillips, P. Riley, and J. W. Griffee (1998), Solar Wind Electron Proton Alpha Monitor (SWEPAM) for the Advanced Composition Explorer, *Space Sci. Rev.*, *86*, 563–612, doi:10.1023/A:1005040232597.

Odstrcil, D., and V. J. Pizzo (1999), Three-dimensional propagation of CMEs in a structured solar wind flow: 1. CME launched within the streamer belt, *J. Geophys. Res.*, *104*, 483–492, doi:10.1029/1998JA900019.

Odstrcil, D., and V. J. Pizzo (2002), Numerical simulation of interplanetary disturbances, in *Solspa 2001: Proceedings of the Second Solar Cycle and Space Weather Euroconference*, edited by H. Sawaya-Lacoste, *Eur. Space Agency Spec. Publ.*, *ESA-SP 477*, 281–284.

Ogilvie, K. W., and M. D. Desch (1997), The wind spacecraft and its early scientific results, *Adv. Space Res.*, *20*, 559–568.

Ogilvie, K. W., et al. (1995), SWE, A comprehensive plasma instrument for the Wind spacecraft, *Space Sci. Rev.*, *71*, 55–77.

Rickett, B. (1992), IPS observations of the solar wind velocity and microscale density irregularities in the inner solar wind, in *Solar Wind Seven*, edited by E. Marsch and R. Schwenn pp. 255–258, Pergamon, New York.

Stone, E. C., A. M. Frandsen, R. A. Mewaldt, E. R. Christian, D. Margolies, J. F. Ormes, and F. Snow (1998), The Advanced Composition Explorer, *Space Sci. Rev.*, *86*(1–22), doi:10.1023/A:1005082526237.

Tóth, G., and D. Odstrcil (1996), Comparison of some flux corrected transport and total variation diminishing numerical schemes for hydrodynamic and magnetohydrodynamic problems, *J. Comput. Phys.*, *128*, 82.

Wenzel, F. P., R. G. Marsden, D. E. Page, and E. J. Smith (1992), The ULYSSES mission, *Astron. Astrophys. Suppl. Ser.*, *92*, 207.

Zhang, J., et al. (2007), Solar and interplanetary sources of major geomagnetic storms ($Dst \leq -100$ nT) during 1996–2005, *J. Geophys. Res.*, *112*, A10102, doi:10.1029/2007JA012321. (Correction, *J. Geophys. Res.*, *112*, A12103, doi:10.1029/2007JA012891.)

M. M. Bisi, A. Buffington, J. M. Clover, P. P. Hick, and B. V. Jackson, Center for Astrophysics and Space Sciences, University of California, San Diego, 9500 Gilman Drive #0424, La Jolla, CA 92093-0424, USA. (mmbisi@ucsd.edu)

D. Odstrcil, Cooperative Institute for Research in Environmental Sciences, University of Colorado, 216 UCB, Boulder, CO 80309-0216, USA.